

**Higher-order topological superconductors characterized by Fermi level crossings**Hong Wang  and Xiaoyu Zhu <sup>\*</sup>*School of Physics, MOE Key Laboratory for Non-equilibrium Synthesis and Modulation of Condensed Matter, Xi'an Jiaotong University, Xi'an, Shaanxi 710049, China*

(Received 17 March 2023; revised 8 September 2023; accepted 8 September 2023; published 20 September 2023)

We demonstrate that level crossings at the Fermi energy serve as robust indicators for higher-order topology in two-dimensional superconductors of symmetry class D. These crossings occur when the boundary condition in one direction is continuously varied from periodic to open, revealing the topological distinction between opposite edges. The associated Majorana numbers acquire nontrivial values whenever the system supports two Majorana zero modes distributed at its corners. Owing to their immunity to perturbations that break crystalline symmetries, Fermi level crossings are able to characterize a wide range of higher-order topological superconductors. By directly identifying the level-crossing points from the bulk Hamiltonian, we establish the correspondence between gapped bulk and Majorana corner states in higher-order phases. In the end, we illustrate this correspondence using two toy models. Our findings suggest that Fermi level crossings offer a possible avenue for characterizing higher-order topological superconductors in a unifying framework.

DOI: [10.1103/PhysRevB.108.125426](https://doi.org/10.1103/PhysRevB.108.125426)**I. INTRODUCTION**

Topological states of matter are usually endowed with a bulk-boundary correspondence, which facilitates the identifications of topologically protected gapless boundary modes without going into the details of the energy spectrum at open boundaries [1–3]. Recent advancements in higher-order topological systems have extended this correspondence to include gapped boundaries [4–13], with gapless corner (hinge) modes appearing at the intersections of adjacent edges (surfaces). Tremendous efforts have been devoted to classifying and characterizing these topological states, mostly in crystalline-symmetry-protected systems [14–34]. However, it is well known that gapless corner or hinge states persist when crystalline symmetries are broken. This is especially evident in higher-order topological superconductors [35–40], where Majorana zero modes [41–46] remain stable as midgap states unless the bulk or boundary gap closes. Hence it would be desirable to characterize higher-order states regardless of whether crystalline symmetries are present.

Higher-order topology can be understood from a boundary perspective, as different parts of the whole boundary, such as the four edges of a square lattice, may exhibit a distinct topology in higher-order phases. For intrinsic higher-order states, the relevant crystalline symmetry requires symmetry-related edges or surfaces to be topologically inequivalent [14–16]. A topology change is only possible through bulk-gap closing. Consequently, bulk invariants, such as symmetry indicators related to the crystalline symmetry, can be defined [17–20]. This stands in contrast with boundary-obstructed topological states, which fall within an extrinsic higher-order classification [11,40]. Without the protections of crystalline symmetries, the boundary topology in these states could

change while the bulk gap remains open. One may characterize the topology by Wilson loop eigenvalues of Wannier bands that are obtained from Wilson loops of energy bands, the so-called nested Wilson loop approach [4,5]. However, the quantization of such topological invariants still requires the presence of crystalline symmetries, such as mirror symmetry [11,38]. Establishing bulk-boundary correspondence under broken crystalline symmetries remains an open question. Considering that boundary topology is ultimately determined by the bulk properties for both intrinsic and boundary-obstructed phases, it should be possible to associate a topological invariant with it based on bulk information, which applies in both phases.

In this paper, we focus on two-dimensional (2D) superconductors of symmetry class D [3] and higher-order phases featuring two Majorana corner states. The higher-order topology can be characterized by a pair of Majorana numbers, which are intimately related to Fermi level crossings that emerge during the continuous variation of the boundary condition along one direction, as illustrated in Fig. 1(a). We further introduce a generic method for locating these crossings from the bulk Hamiltonian. As a result, bulk-boundary correspondence is established in both higher-order phases discussed earlier, due to the robustness of the Fermi level crossings against crystalline-symmetry-breaking perturbations.

**II. GENERAL THEORY**

To demonstrate how Fermi level crossings determine the higher-order topology of D-class superconductors, we start from a 2D periodic lattice and modulate its boundary condition in one direction. The resulting Bogoliubov–de Gennes (BdG) Hamiltonian can be expressed as

$$\tilde{\mathcal{H}}_{\lambda_a} = \sum_{k_a} \mathcal{H}_{\lambda_a}(k_a) = \tilde{\mathcal{H}}_1 - (1 - \lambda_a) \sum_{k_a} \mathcal{B}_a(k_a), \quad (1)$$

<sup>\*</sup>xiaoyu.zhu@xjtu.edu.cn

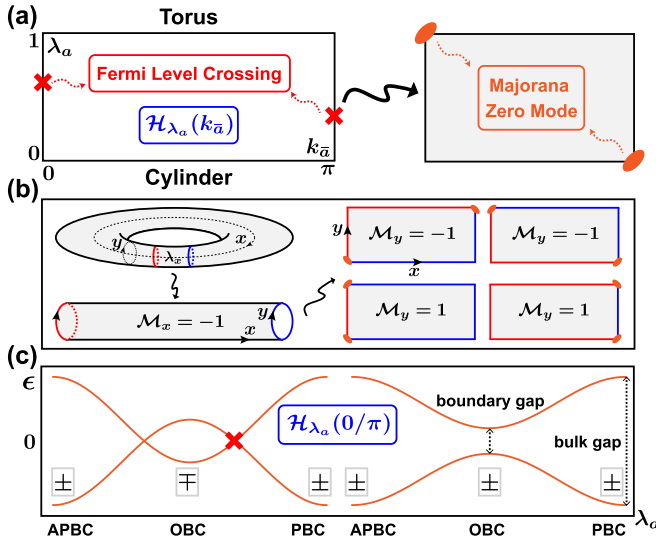


FIG. 1. (a) Higher-order topology characterized by Fermi level crossings in the D symmetry class. Crossings occur at high-symmetry momenta  $K = 0, \pi$ , when the system on a torus ( $\lambda_a = 1$ ) is continuously deformed into a cylinder ( $\lambda_a = 0$ ). (b) Topology of edges determined by Majorana numbers. When  $\mathcal{M}_{x(y)} = -1$ , two opposite edges along the  $y(x)$  direction exhibit a distinct topology, indicated by different colors. (c) Schematic plots of the BdG spectrum at  $K = 0(\pi)$  with or without level crossings. The fermion parity of the ground state (“+” for even, “-” for odd) switches at each crossing. The crossing may disappear when the bulk or boundary gap closes.

where  $\bar{a} = y(x)$  when  $a = x(y)$ , and the real parameter  $\lambda_a$  controls the boundary condition in the  $a$  direction, with  $\lambda_a = 1, -1, 0$  corresponding to the periodic (PBC), antiperiodic (APBC), and open boundary condition (OBC), respectively. In Eq. (1),  $\mathcal{H}_{\lambda_a}(k_{\bar{a}})$  represents the 1D boundary-modulated Hamiltonian at wave vector  $k_{\bar{a}}$ , and  $\mathcal{B}_a(k_{\bar{a}})$  involves all terms that cross its boundary. The lattice terminations we consider are compatible with unit cells, thus allowing the specific form of  $\mathcal{B}$  to be directly read off from the bulk Hamiltonian  $\tilde{\mathcal{H}}_1$ . The process of varying  $\lambda_a$  from 1 to 0 is akin to gradually cutting a torus along the  $\bar{a}$  direction until it eventually becomes a cylinder, as illustrated in Fig. 1(b) for the case of  $a = x$ .

Here, we consider a gapped bulk with trivial first-order topology, which means the cylindrical system described by  $\tilde{\mathcal{H}}_{\lambda_a=0}$  is fully gapped. Treating it as a quasi-1D system along the  $\bar{a}$  direction, we may characterize the higher-order topology with the Majorana number [47–49]

$$\mathcal{M}_a = \text{sgn} \prod_K \text{Pf}[-iH_{\lambda_a=0}(K)], \quad (2)$$

where “Pf” is shorthand for Pfaffian,  $K = 0, \pi$  represents the high-symmetry momentum, and  $H$  refers to the matrix representation of  $\mathcal{H}$  in the Majorana basis. In 1D, the Majorana number being  $-1$  implies the presence of a single Majorana zero mode at each end. If either  $\mathcal{M}_x$  or  $\mathcal{M}_y$ , or both of them, take the value of  $-1$ , we will instead have two Majorana zero modes at the corners of a 2D sheet. To elaborate this let us consider the cylindrical system in the lower left-hand panel of Fig. 1(b) with  $\mathcal{M}_x = -1$ . If we cut it along the axis, the

resulting two edges along the  $x$  direction will each harbor one Majorana mode. Due to the trivial first-order topology, these localized modes cannot propagate along the edges and must be confined to their respective ends, i.e., the corners. If, in addition  $\mathcal{M}_y = -1$ , the two modes would also appear at the two edges in the  $y$  direction. As a result, they can only reside at opposite corners, as depicted in the upper right-hand panel of Fig. 1(b). If  $\mathcal{M}_y = 1$ , however, they would appear at adjacent corners along the  $y$  direction, as shown in the lower right-hand panel of Fig. 1(b).

The Majorana number defined in Eq. (2) is closely related to level crossings at the Fermi energy  $\epsilon = 0$  that appear while  $\lambda_a$  varies in the range  $[0, 1]$ . Notably, Eq. (2) only involves the 1D Hamiltonian at high-symmetry momenta  $K$ . Therefore, we only need to consider Fermi level crossings in these subsystems, as shown in Fig. 1(a). At each crossing, the fermion parity of the ground state switches, indicated by the sign change of  $\text{Pf}[-iH_{\lambda_a}(K)]$ . We can then characterize the fermion-parity difference between PBC and OBC by the number of crossings in between, denoted by  $\eta_{a,K}$ , as Fig. 1(c) demonstrates. This is formally expressed as

$$(-1)^{\eta_{a,K}} = \frac{\text{sgn} \text{Pf}[-iH_{\lambda_a=0}(K)]}{\text{sgn} \text{Pf}[-iH_{\lambda_a=1}(K)]}. \quad (3)$$

We may also define a Majorana number for the toroidal system  $\tilde{\mathcal{H}}_{\lambda_a=1}$  ( $\tilde{\mathcal{H}}_1$ ) similar to Eq. (2), which due to trivial first-order topology must be positive, i.e.,

$$\text{sgn} \prod_K \text{Pf}[-iH_{\lambda_a=1}(K)] = 1. \quad (4)$$

Combining Eqs. (2)–(4), we arrive at

$$\mathcal{M}_a = \prod_K (-1)^{\eta_{a,K}} = (-1)^{\eta_a}, \quad (5)$$

where  $\eta_a$  denotes the total number of crossings at  $K = 0, \pi$ . An odd value of  $\eta_x$  or  $\eta_y$  implies the system resides in a higher-order phase. Fermi level crossings are protected by fermion-parity conservation and particle-hole symmetry, making them immune to crystalline-symmetry-breaking perturbations [50].

Intuitively, we may understand the relation between Fermi level crossings and higher-order topology from the viewpoint of boundary topology. As shown in Fig. 1(b), an odd value of  $\eta_a$  ( $\mathcal{M}_a = -1$ ) reveals that opposite edges along  $\bar{a}$  are topologically inequivalent (shown in different colors). This explains the possible locations of Majorana zero modes, which appear at the intersections of topologically distinct edges. In some simple models, as we demonstrate later, the edge topology can be characterized by the sign of the mass gap in the edge Hamiltonian, allowing us to validate this argument.

To establish the bulk-boundary correspondence, we will demonstrate how the Fermi level crossings of the 1D subsystems are identified from the bulk Hamiltonian. For brevity, we use  $\mathcal{H}_\lambda$  to replace  $\mathcal{H}_{\lambda_a}(K)$ , where

$$\mathcal{H}_\lambda = \mathcal{H}_1 - (1 - \lambda)\mathcal{B} \quad (6)$$

represents a generic 1D Hamiltonian of D class. Following the prescription given by Ref. [51], we first define a retarded

Green's function

$$\mathcal{G}_\lambda(\epsilon) = (\epsilon - \mathcal{H}_\lambda + i\delta)^{-1} = \mathcal{A}_\lambda^{-1}(\epsilon)\mathcal{G}_1(\epsilon), \quad (7)$$

where  $\delta$  is a positive infinitesimal,  $\mathcal{G}_1(\epsilon)$  is the Green's function corresponding to the bulk Hamiltonian  $\mathcal{H}_1$ , and  $\mathcal{A}_\lambda(\epsilon) = 1 + (1 - \lambda)\mathcal{G}_1(\epsilon)\mathcal{B}$ . Since we focus on the parameter regime in which the bulk is fully gapped, in-gap states of  $\mathcal{H}_\lambda$  are solely determined by the poles of  $\mathcal{A}_\lambda^{-1}(\epsilon)$ . Consequently, level-crossing points are identified as roots of

$$\det[A_\lambda(\epsilon = 0)] = 0, \quad (8)$$

where  $A_\lambda$  is the matrix representation of  $\mathcal{A}_\lambda$ . As  $\mathcal{B}$  only includes intracell terms crossing the boundary, we then have  $[A_\lambda]_{IJ} = \delta_{IJ}$  if  $J$  does not appear in these terms. This enables us to calculate  $\det(A)$  using a much smaller matrix  $D$ , which is obtained by projecting  $\mathcal{A}$  into the eigenspace of  $\mathcal{B}$  and satisfies  $\det(D) = \det(A)$ . The entries of  $D$  are given by

$$[D_\lambda(\epsilon)]_{ij} = \delta_{ij} + (1 - \lambda) \sum_{n,k} \frac{\langle i|n, k\rangle \langle n, k|\mathcal{B}|j\rangle}{\epsilon - \epsilon_{n,k}}, \quad (9)$$

where  $\epsilon_{n,k}$  denotes the energy spectrum of the bulk Hamiltonian  $\mathcal{H}_1$  in the Brillouin zone, with  $|n, k\rangle$  being the corresponding eigenstate, and  $|i\rangle, |j\rangle$  represent the eigenvectors of  $\mathcal{B}$ . The dimension of  $D_\lambda$  is equal to the rank of  $\mathcal{B}$ , denoted by  $N_b$ . We then obtain the characteristic equation

$$\det[D_\lambda(\epsilon = 0)] = 0, \quad (10)$$

which has  $N_b$  roots in total. The number of Fermi level crossings  $\eta$  is half the number of real roots in the interval  $[0,1]$ , from which we can readily obtain Majorana numbers according to Eq. (5).

Compared to Eq. (2), where Majorana numbers are determined by calculating the Pfaffian of finite systems with open boundaries [52], i.e.,  $\text{Pf}[-iH_{\lambda_0=0}(K)]$ , and the accuracy crucially depends on system size, identifying the Fermi level crossings is computationally more accurate and efficient for a translation-invariant system. It does not suffer from finite-size effects, and the computational cost is similar to Wilson loop calculations. Moreover, it provides a potential path to characterizing higher-order topological superconductors in other symmetry classes such as the DIII or BDI classes, where Fermi level crossings might be protected by their topological charges. Additionally, by pinpointing the crossings directly from the bulk Hamiltonian, we establish the correspondence between gapped bulk and gapless corner states in higher-order phases. In the following, we shall illustrate this in specific models.

### III. TOY MODELS

First, we consider a two-leg Kitaev ladder [53–56] as schematically shown in Fig. 2(a), and demonstrate how level crossings are identified from the bulk Hamiltonian. Each unit cell contains four Majorana fermions denoted by  $\alpha_{s,j}$  and  $\beta_{s,j}$ , with  $s = 1, 2$  being the chain index and  $j$  referring to the cell index. The boundary-modulated Hamiltonian with  $N$  unit cells has the form  $\mathcal{H}_\lambda = \Gamma^T H_\lambda \Gamma$  in the Majorana basis  $\Gamma = \bigoplus_{j=1}^N \Gamma_j$ , where  $\Gamma_j = \{\alpha_{1,j}, \alpha_{2,j}, \beta_{1,j}, \beta_{2,j}\}^T / \sqrt{2}$

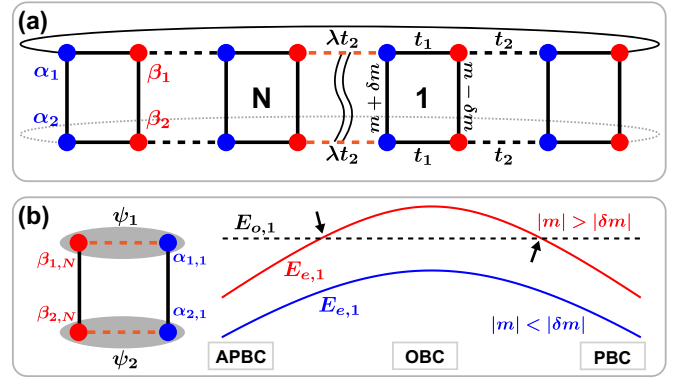


FIG. 2. (a) Geometry of the two-leg Kitaev ladder.  $\lambda$  controls the boundary condition. (b) The fermion-parity switch in a dimerized lattice ( $t_1 = 0$ ). For the case of  $|m| > |\delta m|$ , the ground state switches from the even-parity sector ( $E_{e,1}$ , solid lines) to the odd-parity sector ( $E_{o,1}$ , dashed lines) while the boundary condition varies from PBC (APBC) to OBC. Level crossings are indicated by black arrows.

and the Hamiltonian matrix is given by

$$H_\lambda = \sum_{r=0,\pm 1} T^r \otimes h_r + \lambda(T^{N-1} \otimes h_1^\dagger + \text{H.c.}). \quad (11)$$

Here,  $T$  denotes the translation operator that moves each cell by one site to the left, with  $T|j\rangle = |j-1\rangle$  and  $T|j=1\rangle = 0$  [57]. Hamiltonian (11) includes the intracell term  $h_0 = -t_1\tau_y - m\sigma_y - \delta m\tau_z\sigma_y$ , and intercell term  $h_1 = h_{-1}^\dagger = t_2(\tau_y + i\tau_x)/2$ , with  $\tau$  and  $\sigma$  being Pauli matrices that act in the chain and rung space separately.  $t_1$  and  $t_2$  represent couplings of Majorana fermions along the chain, while  $m$  and  $\delta m$  are those along the rung. For brevity, we assume  $t_1$  and  $t_2$  to be non-negative.

In this model,  $m$  and  $\delta m$  determine whether level crossings occur when  $\lambda$  varies in the range  $[0,1]$ . This is readily seen in a perfectly dimerized lattice ( $t_1 = 0$ ), in which case only the boundary block shown in Fig. 2(b) depends on  $\lambda$ , and its Hamiltonian has the form

$$\begin{aligned} \mathcal{H}_b = & -2\lambda t_2(\psi_1^\dagger \psi_1 + \psi_2^\dagger \psi_2 - 1) \\ & + 2i(m\psi_1^\dagger \psi_2 + \delta m\psi_1^\dagger \psi_2^\dagger - \text{H.c.}), \end{aligned} \quad (12)$$

where  $\psi_s = (\alpha_{s,1} + i\beta_{s,N})/2$  are fermionic operators. The conservation of fermion number parity enables us to study the lowest-energy levels in the even- and odd-parity sectors separately, with  $E_{e,1} = -2\sqrt{\lambda^2 t_2^2 + \delta m^2}$  and  $E_{o,1} = -2|m|$ . While the boundary condition goes from PBC to OBC, the two levels would cross if  $0 < m^2 - \delta m^2 < t_2^2$ , signaling a switch in the ground-state fermion parity, as demonstrated in Fig. 2(b). This parity switch could be observed from the zero-bias peak in an experimental setup that consists of two quantum dots coupled by a nanowire-superconductor heterojunction [58,59]. The parameters  $m$  and  $\delta m$  are related to the electrochemical potential of quantum dots, and  $t_2$  or  $\lambda$  is controlled by tuning cross the Andreev reflection and elastic cotunnelling.

For generic  $t_1$ , we have  $\mathcal{H}_1 = \sum_k \Gamma_{-k}^T H_k \Gamma_k$  in  $k$  space, with the basis  $\Gamma_k = \{\alpha_{1,k}, \alpha_{2,k}, \beta_{1,k}, \beta_{2,k}\}^T / \sqrt{2}$ , and the Bloch

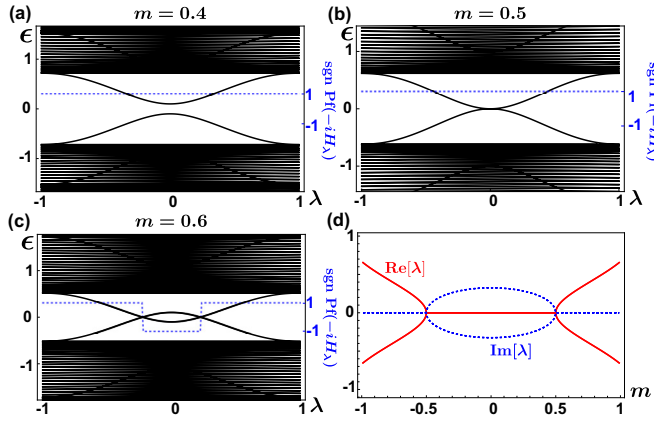


FIG. 3. (a)–(c) Fermi level crossings in a BdG spectrum. The fermion parity switches at each crossing. The crossing appears when  $|m| > |\delta m|$ . Blue dashed lines indicate signs of the Pfaffian of a 1D Hamiltonian. (d) The variation of crossing points  $\lambda$  with  $m$ .  $\delta m = 0.5$ ,  $t_1 = 1$ , and  $t_2 = 2$ .

### Hamiltonian

$$H_k = (-t_1 + t_2 \cos k)\tau_y - t_2 \sin k\tau_x - m\sigma_y - \delta m\tau_z\sigma_y. \quad (13)$$

The energy spectrum is given by

$$\epsilon_{n,k} = \pm \sqrt{t_1^2 + t_2^2 - 2t_1t_2 \cos k + \delta m^2 \pm m}, \quad (14)$$

with  $n$  being the band index. Substituting  $\epsilon_{n,k}$  and  $\mathcal{B} = \Gamma_N^T h_1 \Gamma_1 + \text{H.c.}$  into Eqs. (9) and (10), we obtain

$$\lambda^2 = 1 - \frac{2\Lambda}{\Lambda - a + 2t_2^2}, \quad (15)$$

with  $\Lambda = \sqrt{a^2 - b^2}$ ,  $a = t_1^2 + t_2^2 + \delta m^2 - m^2$ , and  $b = 2t_1t_2$ . From Eq. (15), we find that the number of crossings  $\eta = 1$  when  $0 < m^2 - \delta m^2 < (t_2 - t_1)^2$  and  $t_1 < t_2$ , as shown in Fig. 3. This indicates that the boundary phase transition occurs at  $|m| = |\delta m|$  as in the dimerized case, which is verified by the exact boundary spectrum (see Supplemental Material [60] and Ref. [61] therein). In the special case where  $\delta m = 0$ , Hamiltonian (13) is invariant under inversion, with the corresponding operator being  $\tau_y$ , up to a gauge factor. The inversion symmetry facilitates the direct determination of the Fermi level crossings from the differences of the ground-state inversion eigenvalues between PBC and APBC [60]. With the knowledge of  $\eta$  in a 1D system, we can proceed to determine the higher-order topology in a 2D system, according to Eq. (5).

The 2D Hamiltonian we consider takes the form

$$H_k^{2D} = [t_2(\cos k_x + \cos k_y) - t_1 - t_2]\tau_y - \delta m\tau_z\sigma_y - t_2(\sin k_x\tau_x + \sin k_y\tau_z\sigma_z) - m(\cos \theta\sigma_y + \sin \theta\tau_x\sigma_x), \quad (16)$$

when written in the Majorana basis as in Eq. (13), and reduces to the 1D Hamiltonian at  $k_y = 0$ ,  $\theta = 0$ . This model is equivalent to the  $p \pm ip$  superconductor under an in-plane Zeeman field [62,63]. According to Eq. (5), Majorana numbers  $(\mathcal{M}_x, \mathcal{M}_y)$  are determined by Fermi level crossings of four 1D Hamiltonians,  $\mathcal{H}_{k_a}(K)$ . In Fig. 4(a), we draw the  $(\theta, \delta m)$  phase diagram. Here, the crossings only occur at

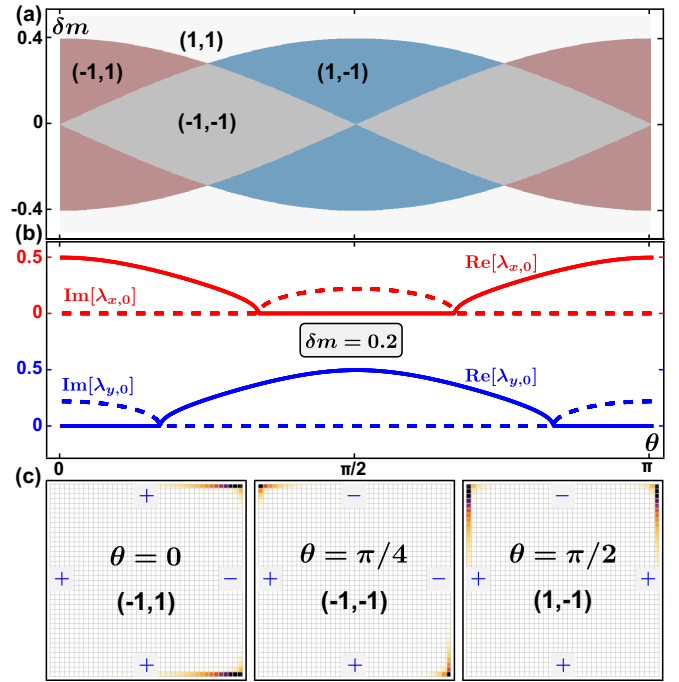


FIG. 4. (a) Phase diagram of the 2D model in  $(\theta, \delta m)$  space. Four different phases are characterized by Majorana numbers  $(\mathcal{M}_x, \mathcal{M}_y)$ . (b) Evolutions of crossing points with  $\theta$ . No crossings appear at  $K = \pi$  in this case and hence only those at  $K = 0$  are displayed. (c) Distributions of Majorana zero modes in three nontrivial phases that are separated by boundary phase transitions. Majorana zero modes appear either at two adjacent corners ( $\theta = 0, \pi/2$ ), or at opposite corners ( $\theta = \pi/4$ ). The symbols “+” and “-” indicate the signs of the edge gaps.  $t_1 = 0.5$ ,  $t_2 = 1$ , and  $m = 0.4$ .

$K = 0$  as Fig. 4(b) shows, although it is possible they emerge at  $K = \pi$  for  $t_1$  and  $t_2$  taking other values. Two Majorana corner states emerge when at least one Majorana number takes  $-1$ , as illustrated in Fig. 4(c).

To corroborate previous arguments concerning the relation between level crossings and boundary topology, we obtain the mass gap for an arbitrary edge [60], given by

$$\Delta(\phi) = \delta m - m \cos(\phi - \theta), \quad (17)$$

where  $\phi$  indicates the normal direction of the edge ( $\phi = 0, \pi/2$  for right and top edges, respectively). The topology of the edges in D-class systems can be characterized by the sign of the mass gap. As seen from the three representative cases in Fig. 4(c), gaps of opposite edges along  $y(x)$  indeed take different signs when  $\eta_{x(y)}$  is an odd number, or equivalently,  $\mathcal{M}_{x(y)} = -1$ . This can be guaranteed when inversion symmetry is enforced, by noting that  $\Delta(\phi) = -\Delta(\phi + \pi)$  in the absence of  $\delta m$ . In this intrinsic higher-order phase, we always have  $\mathcal{M}_x = \mathcal{M}_y = -1$ . Turning on  $\delta m$  breaks inversion symmetry and drives the system into a boundary-obstructed phase, in which process the gap signs do not change immediately, so is the number of Fermi level crossings. We can therefore use Fermi level crossings to characterize the higher-order topology in both phases.

The robustness of Fermi level crossings is also reflected in their persistence under weak disorder or boundary impurities

[60]. While Eqs. (5) and (10) may not be directly applicable due to potential broken translation symmetry, the number of Fermi level crossings remains unchanged. This reinforces their role as a reliable tool to characterize higher-order topological superconductors.

#### IV. CONCLUSION

In conclusion, Fermi level crossings can serve as useful indicators for higher-order topology in the D symmetry class when the nontrivial phase accommodates two Majorana corner states. The applicability of this approach extends beyond the toy models introduced above, as demonstrated in the Supplemental Material [60] for a Rashba bilayer system. The level crossings we consider emerge while the boundary condition continuously varies from PBC to OBC, during which two

opposite edges gradually decouple. An odd number of crossings signals a topological distinction between the two edges. From this point of view, one may consider Fermi level crossings emerging under variations of other twisted boundary conditions [64] when dealing with higher-order phases with four or more Majorana corner states, where one needs to associate the crossings with topological distinctions between neighboring edges.

#### ACKNOWLEDGMENTS

This work was supported by National Science Foundation of China (NSFC) under Grant No. 11704305 and the Innovation Program for Quantum Science and Technology (2021ZD0302400).

- 
- [1] M. Z. Hasan and C. L. Kane, *Colloquium: Topological insulators*, *Rev. Mod. Phys.* **82**, 3045 (2010).
- [2] X.-L. Qi and S.-C. Zhang, *Topological insulators and superconductors*, *Rev. Mod. Phys.* **83**, 1057 (2011).
- [3] C.-K. Chiu, J. C. Y. Teo, A. P. Schnyder, and S. Ryu, *Classification of topological quantum matter with symmetries*, *Rev. Mod. Phys.* **88**, 035005 (2016).
- [4] W. A. Benalcazar, B. A. Bernevig, and T. L. Hughes, *Quantized electric multipole insulators*, *Science* **357**, 61 (2017).
- [5] W. A. Benalcazar, B. A. Bernevig, and T. L. Hughes, *Electric multipole moments, topological multipole moment pumping, and chiral hinge states in crystalline insulators*, *Phys. Rev. B* **96**, 245115 (2017).
- [6] J. Langbehn, Y. Peng, L. Trifunovic, F. von Oppen, and P. W. Brouwer, *Reflection-Symmetric Second-Order Topological Insulators and Superconductors*, *Phys. Rev. Lett.* **119**, 246401 (2017).
- [7] Z. Song, Z. Fang, and C. Fang, *(d - 2)-Dimensional Edge States of Rotation Symmetry Protected Topological States*, *Phys. Rev. Lett.* **119**, 246402 (2017).
- [8] M. Ezawa, *Higher-Order Topological Insulators and Semimetals on the Breathing Kagome and Pyrochlore Lattices*, *Phys. Rev. Lett.* **120**, 026801 (2018).
- [9] F. Schindler, A. M. Cook, M. G. Vergniory, Z. Wang, S. S. P. Parkin, B. A. Bernevig, and T. Neupert, *Higher-order topological insulators*, *Sci. Adv.* **4**, eaat0346 (2018).
- [10] F. Schindler, Z. Wang, M. G. Vergniory, A. M. Cook, A. Murani, S. Sengupta, A. Y. Kasumov, R. Deblock, S. Jeon, I. Drozdov, H. Bouchiat, S. Guéron, A. Yazdani, B. A. Bernevig, and T. Neupert, *Higher-order topology in bismuth*, *Nat. Phys.* **14**, 918 (2018).
- [11] E. Khalaf, W. A. Benalcazar, T. L. Hughes, and R. Queiroz, *Boundary-obstructed topological phases*, *Phys. Rev. Res.* **3**, 013239 (2021).
- [12] Q. Wang, C.-C. Liu, Y.-M. Lu, and F. Zhang, *High-Temperature Majorana Corner States*, *Phys. Rev. Lett.* **121**, 186801 (2018).
- [13] R.-X. Zhang, W. S. Cole, and S. Das Sarma, *Helical Hinge Majorana Modes in Iron-Based Superconductors*, *Phys. Rev. Lett.* **122**, 187001 (2019).
- [14] E. Khalaf, *Higher-order topological insulators and superconductors protected by inversion symmetry*, *Phys. Rev. B* **97**, 205136 (2018).
- [15] M. Geier, L. Trifunovic, M. Hoskam, and P. W. Brouwer, *Second-order topological insulators and superconductors with an order-two crystalline symmetry*, *Phys. Rev. B* **97**, 205135 (2018).
- [16] L. Trifunovic and P. W. Brouwer, *Higher-Order Bulk-Boundary Correspondence for Topological Crystalline Phases*, *Phys. Rev. X* **9**, 011012 (2019).
- [17] A. Skuratovska, T. Neupert, and M. H. Fischer, *Atomic limit and inversion-symmetry indicators for topological superconductors*, *Phys. Rev. Res.* **2**, 013064 (2020).
- [18] S. Ono, H. C. Po, and H. Watanabe, *Refined symmetry indicators for topological superconductors in all space groups*, *Sci. Adv.* **6**, eaaz8367 (2020).
- [19] R. Takahashi, Y. Tanaka, and S. Murakami, *Bulk-edge and bulk-hinge correspondence in inversion-symmetric insulators*, *Phys. Rev. Res.* **2**, 013300 (2020).
- [20] Y.-T. Hsu, W. S. Cole, R.-X. Zhang, and J. D. Sau, *Inversion-protected Higher-order Topological Superconductivity in Monolayer WTe<sub>2</sub>*, *Phys. Rev. Lett.* **125**, 097001 (2020).
- [21] F. Tang, S. Ono, X. Wan, and H. Watanabe, *High-Throughput Investigations of Topological and Nodal Superconductors*, *Phys. Rev. Lett.* **129**, 027001 (2022).
- [22] Z. Yan, *Higher-Order Topological Odd-Parity Superconductors*, *Phys. Rev. Lett.* **123**, 177001 (2019).
- [23] Z. Zhang, J. Ren, Y. Qi, and C. Fang, *Topological classification of intrinsic three-dimensional superconductors using anomalous surface construction*, *Phys. Rev. B* **106**, L121108 (2022).
- [24] A. Bouhon, A. M. Black-Schaffer, and R.-J. Slager, *Wilson loop approach to fragile topology of split elementary band representations and topological crystalline insulators with time-reversal symmetry*, *Phys. Rev. B* **100**, 195135 (2019).
- [25] Y. Hwang, J. Ahn, and B.-J. Yang, *Fragile topology protected by inversion symmetry: Diagnosis, bulk-boundary correspondence, and Wilson loop*, *Phys. Rev. B* **100**, 205126 (2019).
- [26] J. Kruthoff, J. de Boer, J. van Wezel, C. L. Kane, and R.-J. Slager, *Topological Classification of Crystalline Insulators through Band Structure Combinatorics*, *Phys. Rev. X* **7**, 041069 (2017).

- [27] F. Tang, H. C. Po, A. Vishwanath, and X. Wan, Comprehensive search for topological materials using symmetry indicators, *Nature (London)* **566**, 486 (2019).
- [28] T. Zhang, Y. Jiang, Z. Song, H. Huang, Y. He, Z. Fang, H. Weng, and C. Fang, Catalogue of topological electronic materials, *Nature (London)* **566**, 475 (2019).
- [29] M. G. Vergniory, L. Elcoro, C. Felser, N. Regnault, B. A. Bernevig, and Z. Wang, A complete catalogue of high-quality topological materials, *Nature (London)* **566**, 480 (2019).
- [30] R.-X. Zhang, Bulk-Vortex Correspondence of Higher-Order Topological Superconductors, *arXiv:2208.01652*.
- [31] M. Jung, Y. Yu, and G. Shvets, Exact higher-order bulk-boundary correspondence of corner-localized states, *Phys. Rev. B* **104**, 195437 (2021).
- [32] E. Roberts, J. Behrends, and B. Béri, Second-order bulk-boundary correspondence in rotationally symmetric topological superconductors from stacked Dirac Hamiltonians, *Phys. Rev. B* **101**, 155133 (2020).
- [33] S. Kooi, G. van Miert, and C. Ortix, The bulk-corner correspondence of time-reversal symmetric insulators, *npj Quantum Mater.* **6**, 1 (2021).
- [34] S.-J. Huang and Y.-T. Hsu, Faithful derivation of symmetry indicators: A case study for topological superconductors with time-reversal and inversion symmetries, *Phys. Rev. Res.* **3**, 013243 (2021).
- [35] X. Zhu, Second-Order Topological Superconductors with Mixed Pairing, *Phys. Rev. Lett.* **122**, 236401 (2019).
- [36] Z. Yan, F. Song, and Z. Wang, Majorana Corner Modes in a High-Temperature Platform, *Phys. Rev. Lett.* **121**, 096803 (2018).
- [37] T. Liu, J. J. He, and F. Nori, Majorana corner states in a two-dimensional magnetic topological insulator on a high-temperature superconductor, *Phys. Rev. B* **98**, 245413 (2018).
- [38] A. Tiwari, A. Jahin, and Y. Wang, Chiral Dirac superconductors: Second-order and boundary-obstructed topology, *Phys. Rev. Res.* **2**, 043300 (2020).
- [39] Y. Volpez, D. Loss, and J. Klinovaja, Second-Order Topological Superconductivity in  $\pi$ -Junction Rashba Layers, *Phys. Rev. Lett.* **122**, 126402 (2019).
- [40] X. Wu, W. A. Benalcazar, Y. Li, R. Thomale, C.-X. Liu, and J. Hu, Boundary-Obstructed Topological High- $T_c$  Superconductivity in Iron Pnictides, *Phys. Rev. X* **10**, 041014 (2020).
- [41] N. Read and D. Green, Paired states of fermions in two dimensions with breaking of parity and time-reversal symmetries and the fractional quantum Hall effect, *Phys. Rev. B* **61**, 10267 (2000).
- [42] F. Wilczek, Majorana returns, *Nat. Phys.* **5**, 614 (2009).
- [43] J. Alicea, New directions in the pursuit of Majorana fermions in solid state systems, *Rep. Prog. Phys.* **75**, 076501 (2012).
- [44] T. D. Stanescu and S. Tewari, Majorana fermions in semiconductor nanowires: Fundamentals, modeling, and experiment, *J. Phys.: Condens. Matter* **25**, 233201 (2013).
- [45] S. R. Elliott and M. Franz, *Colloquium: Majorana fermions in nuclear, particle, and solid-state physics*, *Rev. Mod. Phys.* **87**, 137 (2015).
- [46] R. Aguado, Majorana quasiparticles in condensed matter, *Riv. Nuovo Cimento* **40**, 523 (2017).
- [47] A. Y. Kitaev, Unpaired Majorana fermions in quantum wires, *Phys. Usp.* **44**, 131 (2001).
- [48] M. Kheirkhah, Z. Yan, and F. Marsiglio, Vortex-line topology in iron-based superconductors with and without second-order topology, *Phys. Rev. B* **103**, L140502 (2021).
- [49] P. P. Poduval, T. L. Schmidt, and A. Haller, Perfectly localized Majorana corner modes in fermionic lattices, *Phys. Rev. B* **108**, 035124 (2023).
- [50] C. W. J. Beenakker, J. M. Edge, J. P. Dahlhaus, D. I. Pikulin, S. Mi, and M. Wimmer, Wigner-Poisson Statistics of Topological Transitions in a Josephson Junction, *Phys. Rev. Lett.* **111**, 037001 (2013).
- [51] J.-W. Rhim, J. H. Bardarson, and R.-J. Slager, Unified bulk-boundary correspondence for band insulators, *Phys. Rev. B* **97**, 115143 (2018).
- [52] M. Wimmer, Algorithm 923: Efficient numerical computation of the Pfaffian for dense and banded skew-symmetric matrices, *ACM Trans. Math. Softw.* **38**, 1 (2012).
- [53] N. Wu, Topological phases of the two-leg Kitaev ladder, *Phys. Lett. A* **376**, 3530 (2012).
- [54] G. Y. Chitov, Local and nonlocal order parameters in the Kitaev chain, *Phys. Rev. B* **97**, 085131 (2018).
- [55] R. Wakatsuki, M. Ezawa, and N. Nagaosa, Majorana fermions and multiple topological phase transition in Kitaev ladder topological superconductors, *Phys. Rev. B* **89**, 174514 (2014).
- [56] Y. Yan, L. Qi, D.-Y. Wang, Y. Xing, H.-F. Wang, and S. Zhang, Topological phase transition and phase diagrams in a two-leg Kitaev ladder system, *Ann. Phys.* **532**, 1900479 (2020).
- [57] A. Alase, E. Cobanera, G. Ortiz, and L. Viola, Exact Solution of Quadratic Fermionic Hamiltonians for Arbitrary Boundary Conditions, *Phys. Rev. Lett.* **117**, 076804 (2016).
- [58] T. Dvir, G. Wang, N. van Loo, C.-X. Liu, G. P. Mazur, A. Bordin, S. L. D. ten Haaf, J.-Y. Wang, D. van Driel, F. Zatelli, X. Li, F. K. Malinowski, S. Gazibegovic, G. Badawy, E. P. A. M. Bakkers, M. Wimmer, and L. P. Kouwenhoven, Realization of a minimal Kitaev chain in coupled quantum dots, *Nature (London)* **614**, 445 (2023).
- [59] A. Bordin, X. Li, D. van Driel, J. C. Wolff, Q. Wang, S. L. D. ten Haaf, G. Wang, N. van Loo, L. P. Kouwenhoven, and T. Dvir, Crossed Andreev reflection and elastic co-tunneling in a three-site Kitaev chain nanowire device, *arXiv:2306.07696*.
- [60] See Supplemental Material at <http://link.aps.org/supplemental/10.1103/PhysRevB.108.125426> for detailed derivations of the boundary spectrum of the two-leg Kitaev ladder; the role of inversion symmetry in determining Fermi level crossings; the effective Hamiltonian for an arbitrary edge in the 2D model; the influence of bulk disorder and boundary impurities on Fermi level crossings; and Fermi level crossings in a Rashba bilayer superconducting system.
- [61] S. S. Pershoguba and V. M. Yakovenko, Shockley model description of surface states in topological insulators, *Phys. Rev. B* **86**, 075304 (2012).
- [62] V. T. Phong, N. R. Walet, and F. Guinea, Majorana zero modes in a two-dimensional  $p$ -wave superconductor, *Phys. Rev. B* **96**, 060505(R) (2017).
- [63] X. Zhu, Tunable Majorana corner states in a two-dimensional second-order topological superconductor induced by magnetic fields, *Phys. Rev. B* **97**, 205134 (2018).
- [64] Z.-D. Song, L. Elcoro, and B. A. Bernevig, Twisted bulk-boundary correspondence of fragile topology, *Science* **367**, 794 (2020).